ICING DISTRIBUTION OF ROTATING BLADE OF HORIZONTAL AXIS WIND TURBINE BASED ON QUASI-3-D NUMERICAL SIMULATION

by

Yan LI[a*], Shaolong WANG[a], Ce SUN[a], Xian YI[b], Wenfeng GUO[a], Zhihong ZHOU[b], and Fang FENG[a]

[a] Heilongjiang Provincial Key Laboratory of Technology and Equipment for the Utilization of Agricultural Renewable Resources in Cold Region, Northeast Agricultural University, Harbin, China
[b] State Key Laboratory of Aerodynamics, China Aerodynamics Research and Development Center, Mianyang, China

Original scientific paper
https://doi.org/10.2298/TSCI170821053L

For researching on the rules of icing distribution on rotating blade of horizontal axis wind turbine, a Quasi-3-D method is proposed to research on icing on rotating blades of horizontal axis wind turbine by numerical simulation. A 2-D and 3-D method of evaluating the irregular shape of ice has been established. The model of rotating blade from a 1.5 MW horizontal axis wind turbine is used to simulate the process and shape of icing on blade. The simulation is carried out under the conditions with four important parameters including ambient temperature, liquid water content, medium volume drop diameter, and icing time. The results reveal that icing mainly happens on 50% ~ 70% of the blade surface along wingspan from tip to root of blade. There are two kinds of icing shapes including horn shape icing and streamline shape icing. The study can provide theoretical basis and numerical reference to development of anti and deicing strategy for wind turbine blades.

Key words: *wind turbine, blade icing, numerical simulation, icing shape, icing shape evaluation*

Introduction

It is well known that wind turbine is widely used in the world because of its clean and no pollution. The countries that have abundant wind energy and well utilization on wind turbine mainly locate in the northern hemisphere. These countries face a common climate problem that is low temperature climate with icing conditions [1]. The influences of icing on wind turbine blade are: The output power of wind turbine decreases and the wind turbine may stop when it is damaged by icing [2, 3]. The load distribution of blade changes and accelerates the fatigue of material. Icing may cause safety accident when wind turbine yaws and changes angle of attack under this condition [4]. The safety of persons and buildings nearby wind turbine may be threatened [5]. A task project is entitled *19* and named *Wind Energy in Cold Climat*e by International Energy Agency in Wind Energy Commission. It commits to solve the problems that wind turbine faces in cold climate [6].

The research on icing mechanism and icing distribution on blade of wind turbine is the fundamental study, especially on rotating one. Establishing a scientific and reasonable eval-

* Corresponding author, e-mail: liyanneau@163.com

uation system of icing on wind turbine is a basis to study icing prevention, hazard assessment and anti-deicing system. Numerical simulation of icing developed rapidly and acquires a lot of research results with rapid developments of computational fluid mechanics, computational heat transfer, and computational mass transfer. Yi *et al*. [7] calculated the water droplets collection rate of large horizontal axis wind turbine and process of freezing by co-ordinate transformation. Jasinski *et al*. [8] simulated the icing on S809 air-foil by Lewice. Han *et al*. [9] obtained the shape of icing by Lewice and compared with the one on rotating blade that obtained by icing experiment. Ruff [10] researched the ice accretion shapes on air-foils. Hmola *et al*. [11] analyzed the performances of blade before and after icing by TURBOICE under different conditions. Zhu *et al*. [12] studied the simulation of icing on blade air-foil of wind turbine. Deng *et al*. [13] simulated the trajectory of water droplets by the method of fourth-order Runge-Kutta. Li *et al*. [14] studied the icing on blade of vertical axis wind turbine [14].

In this paper simulation of icing on rotating blade of large horizontal axis wind turbine is talked about. The research explore new theory and method of icing on blade of wind turbine by numerical simulation which is based on the previous research results. The findings reveal the distribution of icing on rotary blade of horizontal axis wind turbine. The rules provide the theoretical basis and numerical reference to development of anti and deicing strategy for wind turbine blades.

Model and method

Model

The model of a horizontal axis wind turbine whose output power is 1.5 MW. The diameter of it is 83 m. The diameter of hub is 4.6 m and the length of blade is 39.2 m. Blades of the wind turbine are made of glass fiber reinforced plastic.

Several typical cross-sections of air-foils from wind turbine blade are selected in this paper for simulation. In order to establish a rule of icing for all size of blades, the location of cross-section (r) of air-foil is expressed by percentage ($2r/D$) from hub to cross-section.

The positions of each air-foil are shown in fig. 1. Transforming the 3-D blade into 2-D air-foil based on blade element theory is shown in fig. 2. As shown in fig. 2, the flow velocity is U_∞, the tangential velocity of air-foil is $V = r\omega$ and the resultant velocity is W. For simplifying simulation, as shown in fig. 3, the resultant velocity, W, is leveled by rotating the air-foil and the rotation angle is ψ. By this way the 3-D rotating model of rotating blade is simplified into a 2-D air-foil used for numerical simulation.

The rated parameters of wind turbine are: rated wind speed is 11 m/s, the cut-in wind speed is 3 m/s, the cut-out wind speed is 25 m/s, and rated rotation speed is 20 rpm. The parameters of each air-foil of the blade working at rated power are shown in tab. 1.

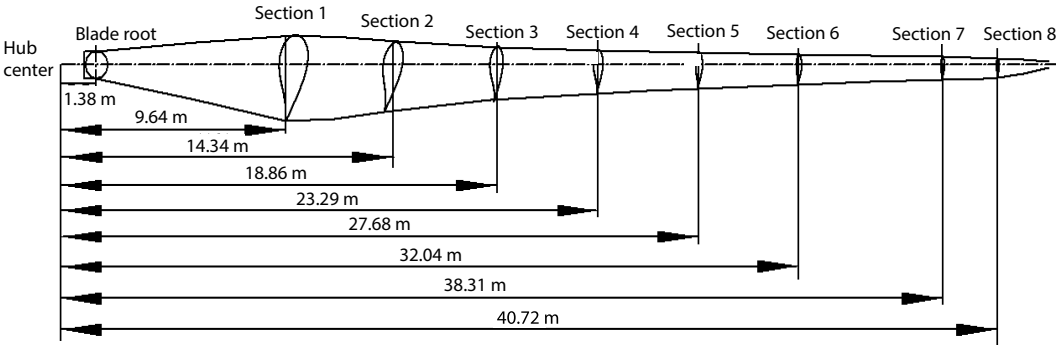

Figure 1. Positions of each air-foil along wingspan

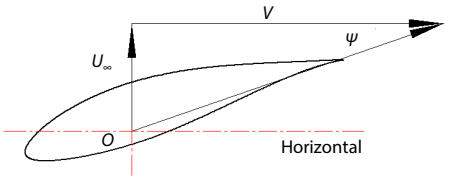

Figure 2. Diagram of velocity vectors

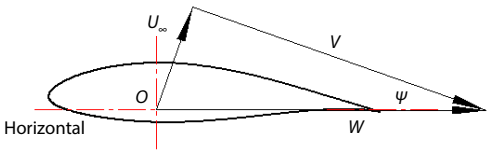

Figure 3. Diagram of transformed velocity vectors

Table 1. Working conditions of each section at rated condition

Section	Cross-section, [%]	r/m	c/m	U_∞ [ms^{-1}]	V [ms^{-1}]	W [ms^{-1}]	ψ [°]
1	23.23	9.64	3.16	11	20.2	23	28.6
2	34.57	14.34	2.58	11	30.05	32	20.1
3	45.44	18.86	2.03	11	39.50	41	15.6
4	56.12	23.29	1.60	11	48.77	50	12.7
5	66.69	27.68	1.33	11	57.97	59	10.8
6	77.20	32.04	1.12	11	67.10	68	9.3
7	92.33	38.31	0.84	11	80.25	81	7.8
8	98.13	40.72	0.69	11	85.29	86	7.3

Method

Simulation method

In this paper, the air-flow field was calculated first. The air-flow field is calculated by N-S equation which has the characteristic of low-velocity viscous flow and solved based on the simple method. The N-S equation is:

$$\frac{\partial \rho \phi}{\partial t} + \nabla(\rho \vec{v} \phi - \Gamma_\phi \text{grad}\phi) = q_\phi \tag{1}$$

where ρ is the air density, ϕ – the transport variable, $\vec{v}$ – the air velocity, Γ_ϕ – the air temperature, and q_ϕ – the source item.

The method bases on the standard turbulence model and the equation is:

$$\frac{\partial \rho k}{\partial t} + \nabla\left[\rho \vec{v} k - \left(\mu_l + \frac{\mu_t}{\sigma_k}\right)\text{grad}k\right] = G_k - \rho\varepsilon + G_b \tag{2}$$

The impingement limit was calculated by the Lalgrangian method and solved based on Runge-Kutta method. The Lagrangian equation is shown:

$$M_d \frac{\text{d}^2 \vec{x}_d}{\text{d}t^2} = (\rho_d - \rho_a) V_d \vec{g} + \frac{1}{2} C_d A_d \rho_a \left|\vec{u}_a - \vec{u}_d\right| (\vec{u}_a - \vec{u}_d) \tag{3}$$

where $\vec{g}$ is the acceleration of gravity, A_d – the area of water droplet facing wind, V_d – the volume of water droplet, C_d – the drag coefficient, $\vec{u}_a$ – the local wind velocity and $\vec{u}_d$ – the water droplet velocity.

The Runge-Kutta equation is:

$$\vec{u}_{n+1} = \vec{u}_n + \frac{1}{6}(t_{n+1} - t_n)(K_1 + 2K_2 + 2K_3 + K_4) \tag{4}$$

Based on the control body theory, the process of icing which droplets impact on blade is solved by mass and energy conservation equations. The principal of mass and energy conservation on the surface of single control body is shown in figs. 4 and 5.

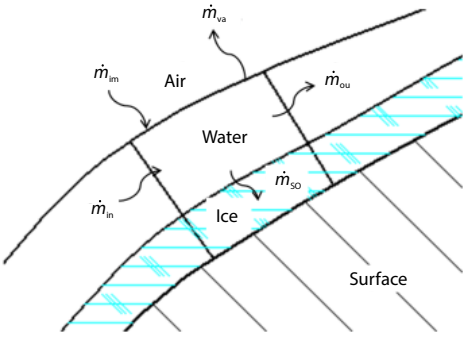

Figure 4. Mass conservation in single control body

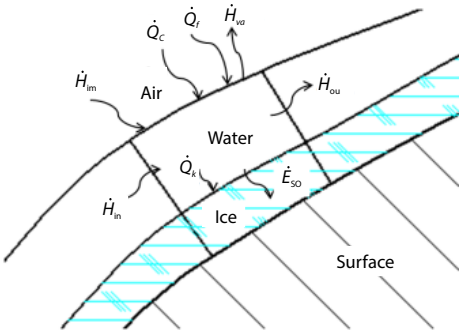

Figure 5. Energy conservation in single control body

According to the mass conservation, the weight of current control body equals to the difference between mass of water going into the surface of control body and the leaving ones. The equation is:

$$\dot{m}_{\mathrm{in}} + \dot{m}_{\mathrm{im}} - \dot{m}_{\mathrm{va}} - \dot{m}_{\mathrm{ou}} = \dot{m}_{\mathrm{so}} \tag{5}$$

The eq. (1) is usually given:

$$\dot{m}_{\mathrm{ou}} = (1-f)(\dot{m}_{\mathrm{im}} + \dot{m}_{\mathrm{in}}) - \dot{m}_{\mathrm{va}} \tag{6}$$

where $\dot{m}_{in}$ is the mass of water flow from upstream into control body, $\dot{m}_{im}$ – the super-cooled droplets impacting on the blade, $\dot{m}_{va}$ – the mass of water transforming into steam by evaporation or sublimation, $\dot{m}_{ou}$ – the mass of water droplets which is not freezes and flow into downstream, $\dot{m}_{so}$ – the mass of water which was changed to ice, and f – the icing ratio.

The surface energy of the control body is subdivided into eight items. According to the first law of thermodynamics, the energy balance equation is:

$$\dot{E}_{\mathrm{so}} + \dot{H}_{\mathrm{va}} + \dot{H}_{\mathrm{ou}} - \dot{H}_{\mathrm{in}} - \dot{H}_{\mathrm{im}} = \dot{Q}_{\mathrm{f}} - \dot{Q}_{\mathrm{c}} - \dot{Q}_{\mathrm{k}} \tag{7}$$

where $\dot{E}_{so}$ is the energy of water during freezing, $\dot{H}_{va}$ – the heat of evaporation of water droplets or ice surface, $\dot{H}_{ou}$ – the energy of droplets out the body, $\dot{H}_{in}$ – the energy of droplets into the body, $\dot{H}_{im}$ – the impact kinetic energy into the water heat flux, $\dot{Q}_f$ – the energy of air friction heating, $\dot{Q}_c$ – the convective hot flow of wall and the environment, and $\dot{Q}_k$ – the heat between ice and water.

Meshing and conditions

In this paper, the simulation software has been developed based on previous theory and the selected air-foil have been meshed finely as shown in fig. 6. The structure and scope of flow field for meshing are shown in fig. 6(a). The result of meshing is shown in fig. 6(b). The grids around the air-foil encrypted and represented such as No. 1 are shown in fig. 6(c). The working conditions are shown in tab. 2.

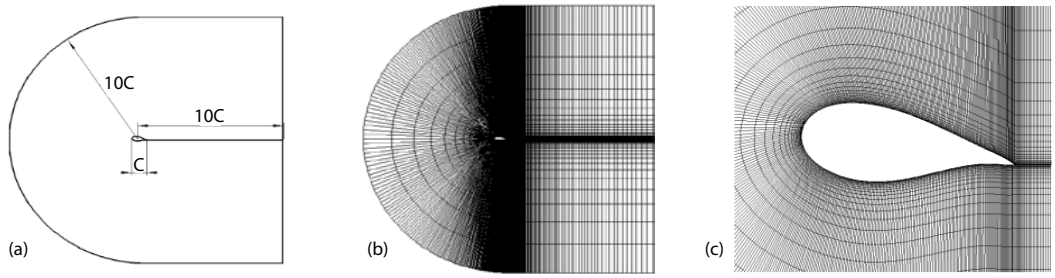

Figure 6. Meshing results; (a) parameters of meshing, (b) result of meshing, (c) meshing of No. 1 air-foil

Table 2. Experimental parameters for simulation

Number of working conditions	T [°C]	LWC [gm^{-3}]	MVD [μm]	Icing time [min]
1	–4	0.1	15	30 60 90 120
2	–8	0.1	15	
3	–12	0.1	15	
4	–4	0.3	15	
5	–8	0.3	15	
6	–12	0.3	15	
7	–4	0.5	15	
8	–8	0.5	15	
9	–2	0.5	15	
10	–4	0.1	30	
11	–8	0.1	30	
12	–12	0.1	30	
13	–4	0.3	30	
14	–8	0.3	30	
15	–12	0.3	30	
16	–4	0.5	30	
17	–8	0.5	30	
18	–12	0.5	30	
19	–4	0.1	45	
20	–8	0.1	45	
21	–12	0.1	45	
22	–4	0.3	45	
23	–8	0.3	45	
24	–12	0.3	45	
25	–4	0.5	45	
26	–8	0.5	45	
27	–12	0.5	45	

Results and discussion

Icing shape and distribution

According to the results obtained by simulation. The icing shapes are classified into two types. One type is the horn icing shape and another is streamlined icing shape. The streamlined icing shape is shown in fig. 7. It has simple shape and smooth contour. The horn icing shape is shown in fig. 8. It has complex shape which has two horns (the upper one and the lower

one). The two horns are a little farther than the central part of ice from air-foil surface. In this study, the horn icing shape happens in the working conditions of No. 2, No. 3, No. 6, No. 11, No. 12, No. 20, and No. 21 from tab. 2. The streamlined icing shape happens in other conditions. The streamlined icing shape in the condition 3 and the horn icing shape in the condition 27 are shown in figs. 7 and 8, respectively.

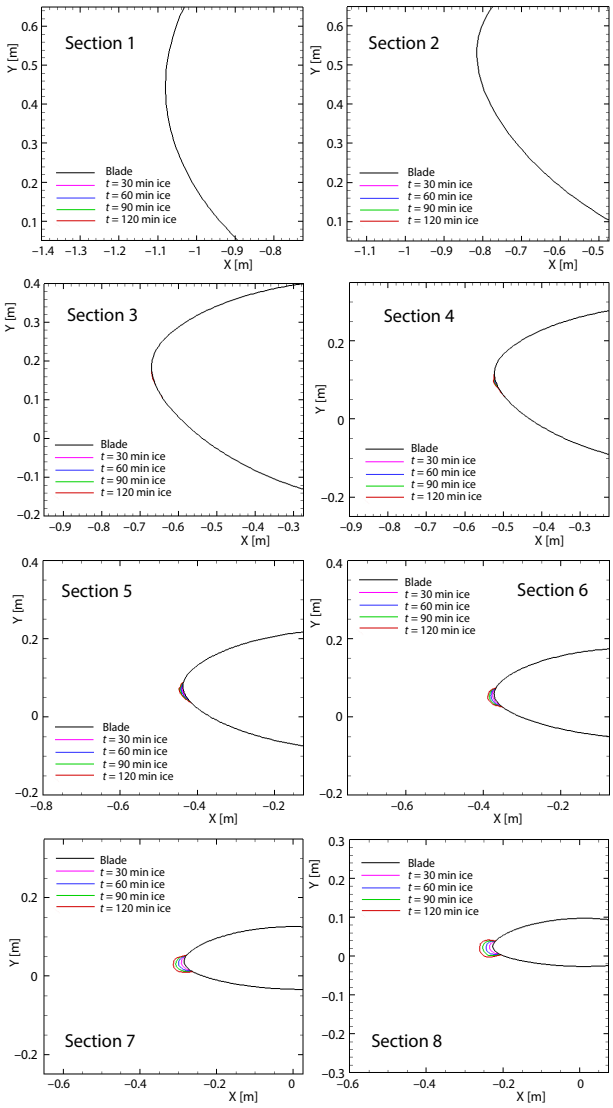

Figure 7. Streamlined icing shape under working condition No. 3

The 3-D icing shape on blade is shown in fig. 9. The model of icing is acquired by the method of Quasi-3-D numerical simulation. According to the results of simulation, the farther location of cross-section is, the larger irregular icing shape is. The reason is that the farther the section is from hub, the higher the linear speed is. Then more water droplets are captured by air-foil in unit time, so the ice shape is larger. The icing area mainly locates at the 50% ~ 70% of blade surface along wingspan from tip to the hub.

With increasing of icing time, the icing shape on blade has no significant change at the same cross-section of air-foil along wingspan and just the amount of icing increases. In the working conditions of No. 2, No. 3, No. 6, No. 11, No. 12, No. 20, and No. 21 from tab. 2, the type of icing is streamlined icing shape and the liquid water content (LWC) in these working conditions is 0.1 g/m^3 except working condition of No. 6 whose LWC is 0.3 g/m^3. In other working conditions the type of icing is horn icing shape and the values of LWC are from 0.3-0.5 g/m^3. With increasing of medium volume drop (MVD) the icing area gradually expands towards to the root of blade. It concludes that MVD only influences the maximum scope of icing area caused by water droplets impacting on blade, but has a little effect on process of icing. In summary, the icing shape is influenced by the ambient temperature and LWC. It can be predicted by these two parameters. The icing shape is determined by LWC and the scope of icing on blade is determined by MVD.

Main parameters of icing shape

Definition of main parameters of two dimensional icing shape

The parameters used to evaluate 2-D icing shape on air-foil are shown in figs. 10 and 11. According to fig. 10, the typical characteristics for evaluating streamlined icing shape include icing area, S, stationary thickness, σ, stationary point deflect angle, θ, icing upper limit, L_u, icing lower limit, L_d, and width of icing, w. According to fig. 11, the typical characteristics of horn icing shape are same with the ones of streamlined icing shape with exception of thickness of upper horn, σ_u, thickness of lower horn, σ_d, deflection angle of upper horn, θ_u, and deflection angle of lower horn, θ_d.

In this paper, the parameters of evaluating icing shape are icing area, S, the maximum stagnation thickness, σ, and volume of icing, V.

The maximum thickness of streamlined icing shape is:

$$\sigma_{max} = \sigma \tag{8}$$

The maximum thickness of horn icing shape is:

$$\sigma_{max} = \max[\sigma, \sigma_u, \sigma_d] \tag{9}$$

According to the results of simulation, the shapes and sizes of icing on different air-foils along wingspan are different. For comparing and analyzing the irregular shapes of icing located at different air-foils, the maximum stationary thickness, σ_{max}, and icing area, S, are non-dimensionless in this paper. The dimensionless parameters are shown:

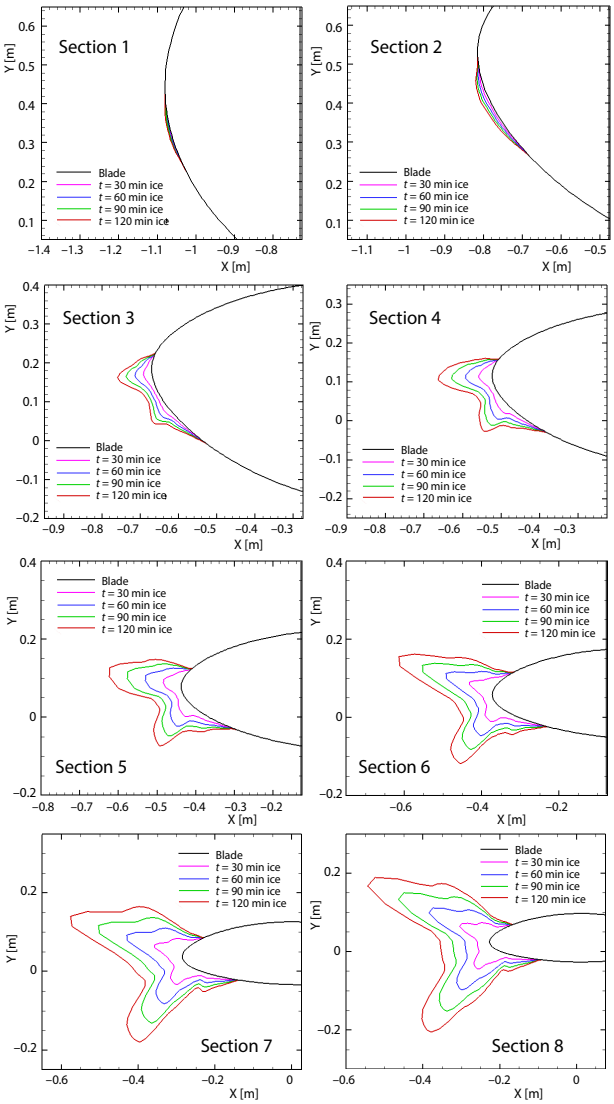

Figure 8. Horn icing shape under working condition No. 27

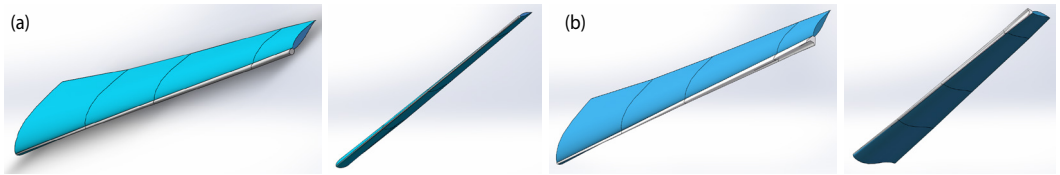

Figure 9. Quasi 3-D shape of icing on blade; (a) streamline ice, (b) horn ice

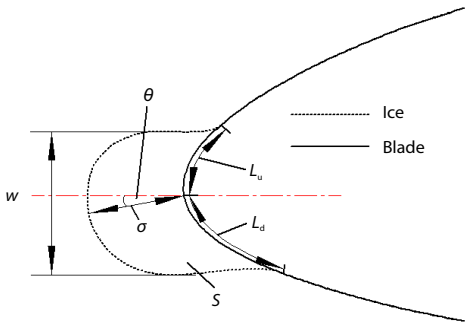

Figure 10. Typical characteristics of streamlined shape ice

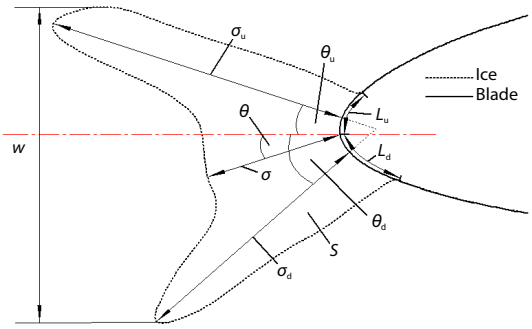

Figure 11. Typical characteristics of horn shape ice

The dimensionless maximum icing area σ_{max} is:

$$\eta_\sigma = \frac{\sigma}{c} \tag{10}$$

The dimensionless maximum thickness of icing μ_s is:

$$\eta_S = \frac{S}{S_b} \tag{11}$$

where S is the surface area of blade and S_b – the surface area of blade.

The maximum icing thickness is 350 mm under the condition of No. 27. The dimensionless maximum icing thicknesses at different cross-sections of air-foils under working condition of No. 25 are shown in figs. 12(a) and 12(b). According to the data and curves in fig. 12, although the maximum thickness of icing at the stationary point increases slightly along wingspan in working condition of No. 25 and decreases at the tip of blade, the dimensionless icing maximum thickness under this condition increases obviously and linearly. It reveals that the shape of air-foil has a significant effect on icing thickness. The air-foil near to the tip of blade has more significant effect on maximum icing thickness.

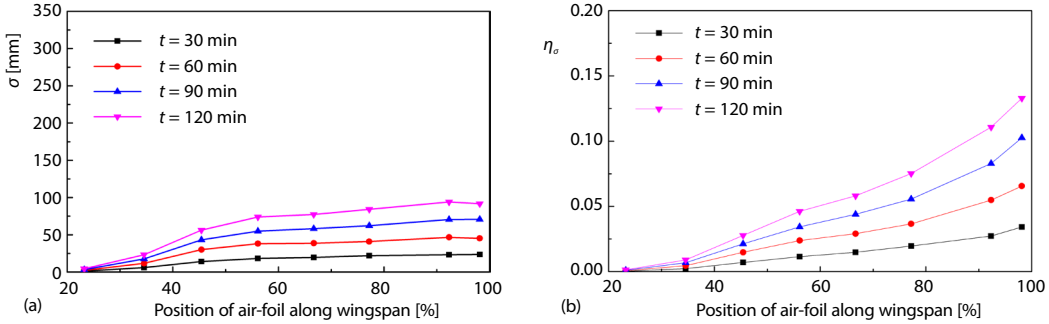

Figure 12. Maximum thicknesses and dimensionless maximum thicknesses along wingspan in condition of No. 25; (a) maximum thickness, (b) dimensionless maximum thickness

The icing areas and dimensionless icing areas in working condition of No. 25 are shown in figs. 13(a) and 13(b). In this condition, the icing area decreases slightly at the tip of blade, but the dimensionless icing area still increases as shown in fig. 13(b). The air-foil near to the tip of blade also has more significant effect on icing area. In other working conditions, the icing area and dimensionless icing area raise linearly with increasing of time.

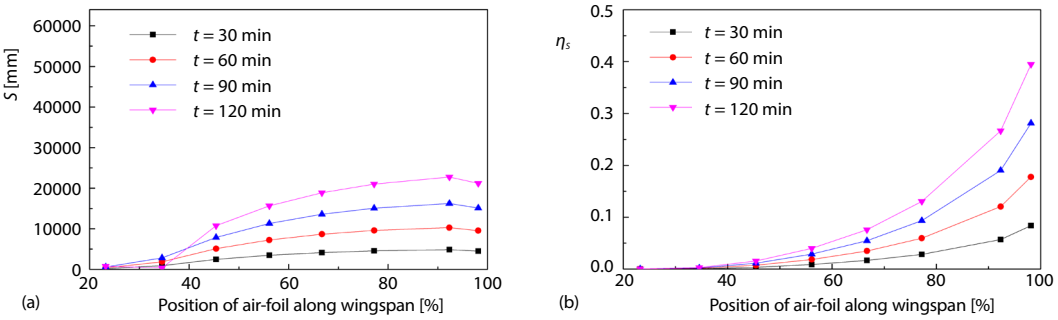

Figure 13. Icing area and dimensionless icing area along wingspan in working condition of No. 25; (a) icing area, (b) dimensionless icing area

Analysis of icing parameters

The volumes of icing in all working conditions are shown in fig. 14. The maximum icing volume is $7.15 \cdot 10^8$ mm^3. It increases linearly along with time and is influenced by LWC and ambient temperature. When LWC is high, the volume of icing reduces with decreasing of ambient temperature. When ambient temperature and MVD are constants, the volume of icing increases with rising of LWC. When ambient temperature and LWC are constants, the volume of icing increases with rising of MVD.

The shapes of air-foils vary at different cross-sections from hub to tip of blade, so the values of typical characteristics are different. In this paper the air-foil of No. 7 is selected to study and analyze the rule of icing on it in all working conditions and the values of typical characteristics are shown in figs. 15 and 16. According to figs. 15 and 16, the icing area and maximum thickness of icing increase linearly along with time. Based on previous analyses the icing area is influenced by ambient temperature and LWC and the rule is similar to the one of icing volume influenced by temperature. Similarly the maximum icing thickness is also influenced by ambient temperature and LWC which obviously influence the shapes of horn icing shape and streamlined icing shape.

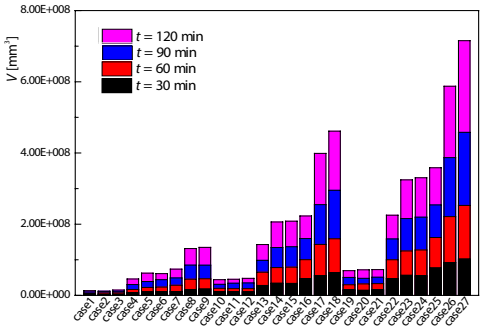

Figure 14. Volumes of different working conditions

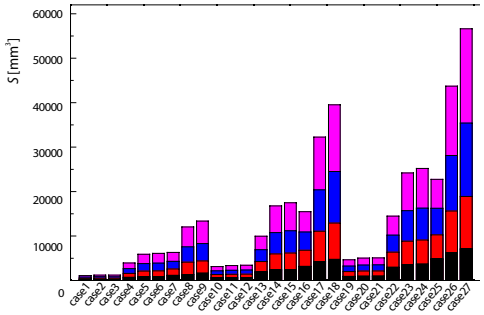

Figure 15. Icing areas of No. 7 air-foil at different working conditions

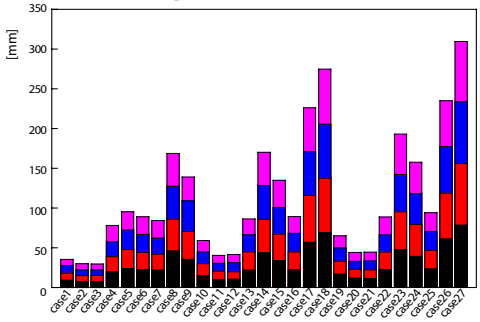

Figure 16. Maximum icing thicknesses of No. 7 air-foil at different working conditions

Conclusions

The main conclusions obtained under the condition of this study are acquired as follows.

- There are two kinds of ice shape on blade air-foil: streamline ice shape and horn ice shape.

The icing seriously occurs at the tip part of blade. The closer to the root is, the less ice generates and the longer the distance from the root is, the more ice generates.

- The environmental temperature and LWC are the two main factors affecting icing on wind turbine. The lower the LWC and the temperature are, the easier super-cool water droplet is to be icing and becomes streamline-ice shape. With increasing of LWC and temperature, the ice accretion has the trend to be horn ice shape.

Acknowledgment

This research was sponsored by the projects supported by National Natural Science Foundation of China (NSFC, No. 51576037 and 11172314) and National Key Basic Research Program of China (2015CB755800). The authors would like to thank to their supports.

Nomenclature

C – chord length, [m]
D – rotor diameter
E – energy, [J]
f – icing ratio
L – icing limit, [mm]
LWC – liquid water content, [gm^{-3}]
MVD – medium volume droplet diameter, [μm]
$\dot{m}$ – mass-flow, [gs^{-1}]
Q – quantity of heat, [J]
S – icing area, [mm^2]
T – icing time, [s]
U_∞ – velocity of wind flows, [ms^{-1}]
V – peripheral speed, [ms^{-1}]
W – resultant velocity, [ms^{-1}]
w – icing width, [mm]

Greek symbols

η – dimensionless method
θ – deflection angle of icing
σ – icing thickness, [mm]
ψ – rotation angle of airfoil, [º]

Subscripts

b – blade
c – convent
d – down icing
in – into
im – impact
k – transfer
max – maximum
ou – out
so – phase change
u – upper icing
va – evaporation

References

[1] Davis, N. N., *et al*., Identifying and Characterizing the Impact of Turbine Icing on Wind Farm Power Generation, *Wind Energy*, *19* (2009), 8, pp. 1503-1518
[2] Wang, Z. J., *et al*., A Light Lithium Niobate Transducer for the Ultrasonic De-Icing of Wind Turbine Blades, *Renewable Energy*, *99* (2016), Dec., pp. 1299-1305
[3] Blasco, P., *et al*., Effect of Icing Roughness on Wind Turbine Power Production, *Wind Energy*, *20* (2017), 4, pp. 601-617
[4] Villalpando, F., *et al*., Prediction of Ice Accretion and Anti-Icing Heating Power on Wind Turbine Blades Using Standard Commercial Software, *Energy*, *114* (2016), Nov., pp. 1041-1052
[5] Lamraoui, F., *et al*., Atmospheric Icing Impact on Wind Turbine Production, *Cold Regions Science and Technology*, *100* (2013), Apr., pp. 36-49
[6] Ville, L., Available Technologies of Wind Energy in Cold Climates, IEA Wind Task, 19, IEA, Paris, 2016
[7] Yi, X., *et al.*, Computation of Icing and its Effect of Horizontal Axis Wind Turbine, *Acta Aerodynamica Sinica*, *35* (2014), 6, pp. 1052-1058
[8] Jasinski, W. J., *et al*., Wind Turbine Performance under Icing Conditions, *Journal of Solar Energy Engineering*, *120* (1998), 1, pp. 60-65
[9] Han, Y. Q., *et al*., Scaled Ice Accretion Experiments on a Rotating Wind Turbine Blade, *Journal of Wind Engineering and Industrial Aerodynamics*, *109* (2012), Oct., pp. 55-67
[10] Ruff, G. A., Quantitative Comparison of Ice Accretion Shapes on Air-foils, *Journal of Aircraft*, *39* (2002), 3, pp. 418-426
[11] Homola, M. C., *et al*., Effect of Atmospheric Temperature and Droplet Size Variation on Ice Accretion of Wind Turbine Blades, *Journal of Wind Engineering and Industrial Aerodynamics*, *98* (2010), 12, pp.724-729

[12] Zhu, C. X., *et al*., Calculation of Wind Turbine Anti-Icing Heat Load, *Journal of Nanjing University of Aeronautics & Astronautics*, *43* (2011), 5, pp. 701-706
[13] Deng, X. X., *et al*., Numerical Simulation of Air-foil Ice Accretion Process on Horizontal-Axis Wind Turbine Blade, *Energy Technology*, *31* (2010), 5, pp. 266-271
[14] Li, Y., *et al*. Characteristics of Ice Accretions on Blade of the Straight-Bladed Vertical Axis Wind Turbine Rotating at Low Tip Speed Ratio, *Cold Regions Science and Technology*, *145* (2018), 13, pp. 1229-1236

Paper submitted: August 21, 2017
Paper revised: November 27, 2017
Paper accepted: November 28, 2017